A Scaler-Based Data Acquisition System for Measuring Parity Violation Asymmetry in Deep Inelastic Scattering

R. Subedi [a 1], D. Wang [a], K. Pan [b], X. Deng [a], R. Michaels [c], P. E. Reimer [d], A. Shahinyan [e], B. Wojtsekhowski [c], X. Zheng [a,*]

[a] *University of Virginia, Charlottesville, VA 22904, USA*

[b] *Massachusetts Institute of Technology, Cambridge, MA 02139, USA*

[c] *Thomas Jefferson National Accelerator Facility, Newport News, VA 23606, USA*

[d] *Physics Division, Argonne National Laboratory, Argonne, IL 60439, USA*

[e] *Yerevan Physics Institute, Yerevan, Armenia*

Abstract

An experiment that measured the parity violating asymmetries in deep inelastic scattering was completed at the Thomas Jefferson National Accelerator Facility in experimental Hall A. From these asymmetries, a combination of the quark weak axial charge could be extracted. To achieve this, asymmetries at the 10^{-4} level needed to be measured at event rates up to 500 kHz and the high pion background typical to deep inelastic scattering experiments needed to be rejected efficiently. A specialized data acquisition (DAQ) system with intrinsic particle identification (PID) was successfully developed and used: The pion contamination in the electron samples was controlled at the order of 2×10^{-4} or below with an electron efficiency of higher than 91% throughout the experiment; the systematic uncertainty in the measured asymmetry due to DAQ deadtime was below 0.2%; and the statistical quality of the asymmetry measurement agreed with the Gaussian distribution to over five orders of magnitudes. The DAQ system is presented here with an emphasis on its design scheme, the achieved PID performance, deadtime effect and the capability of measuring small asymmetries.

Key words: Jefferson Lab; Hall A; PVDIS; DAQ
PACS: 11.30.Er, 12.15.Mm, 13.60.Hb 14.60.Cd 14.65.Bt 29.30.Aj 29.85.Ca

[1] Present address: George Washington University, 725 21^{st} St, NW, Washington, DC 20052, USA

* Corresponding author. E-mail: xiaochao@jlab.org; Telephone: 001-434-243-4032; Fax: 001-434-924-4576

1 Introduction

The Parity Violating Deep Inelastic Scattering (PVDIS) experiment E08-011 was completed in December 2009 at the Thomas Jefferson National Accelerator Facility (JLab). The goal of this experiment [1–3] was to measure with high precision the parity violating asymmetry in deep inelastic scattering of a polarized 6 GeV electron beam on an unpolarized liquid deuterium target. This asymmetry is sensitive to the quark weak axial charge C_{2q} which corresponds to a helicity dependence in the quark coupling with the Z^0 boson.

For electron inclusive scattering from an unpolarized target, the electromagnetic interaction is parity conserving and is insensitive to the spin flip of the incoming electron beam. Only the weak interaction violates parity and causes a difference between the right- and the left-handed electron scattering cross-sections σ_R and σ_L. The dominant contribution to the parity violation asymmetry, $A_{PV} \equiv (\sigma_R - \sigma_L)/(\sigma_R + \sigma_L)$, arises from the interference between electromagnetic and weak interactions and is proportional to the four momentum transfer squared Q^2 for $Q^2 \ll M_Z^2$. The magnitude of the asymmetry is in the order of 10^{-4} or 10^2 parts per million (ppm) at $Q^2 = 1$ (GeV/c)^2.

The PVDIS asymmetry from a deuterium target is

$$A_{PV} = \left(-\frac{G_F Q^2}{4\sqrt{2}\pi\alpha}\right)\left(2g_A^e Y_1 \frac{F_1^{\gamma Z}}{F_1^{\gamma}} + g_V^e Y_3 \frac{F_3^{\gamma Z}}{F_1^{\gamma}}\right) , \tag{1}$$

where Q^2 is the negative of the four-momentum transfer squared, G_F is the Fermi weak coupling constant, α is the fine structure constant, Y_1 and Y_3 are kinematic factors, x is the Bjorken scaling variable, and $F_{1,3}^{\gamma(Z)}$ are deuteron structure functions that can be evaluated from the parton distribution functions and the quark-Z^0 vector and axial couplings $g_{V,A}^q$. From this asymmetry one can extract the quark weak vector and axial charges $C_{1,2q}$, where the quark weak vector charge is defined as $C_{1q} \equiv 2g_A^e g_V^q$ and the quark weak axial charge is given by $C_{2q} \equiv 2g_V^e g_A^q$ with $q = u, d$ indicating an up or a down quark, $g_{A(V)}^e$ is the electron axial (vector) coupling and $g_{V(A)}^q$ is the quark vector (axial) coupling to the Z^0 boson. In the tree-level Standard Model, the $C_{1,2q}$ are related to the weak mixing angle θ_W: $C_{1u} = -\frac{1}{2} + \frac{3}{4}\sin^2\theta_W$, $C_{2u} = -\frac{1}{2} + 2\sin^2\theta_W$, $C_{1d} = \frac{1}{2} - \frac{2}{3}\sin^2\theta_W$, and $C_{2d} = \frac{1}{2} - 2\sin^2\theta_W$. Although the weak mixing angle and the quark weak vector charge C_{1q} have been measured from various processes [4], the current knowledge on the quark weak axial charge C_{2q} is poor and their deviations from the Standard Model value would reveal possible New Physics in the quark axial couplings that could not be accessed from other Standard Model parameters.

The goal of JLab E08-011 was to measure the PVDIS asymmetries to statistical

precisions of 3% and 4% at $Q^2 = 1.1$ and 1.9 (GeV/c)^2, respectively, and under the assumption that hadronic physics corrections are small, to extract the quark axial weak charge combination $(2C_{2u} - C_{2d})$. In addition, the systematic uncertainty goal was less than 3%. For this experiment, the expected asymmetries were 91 and 160 ppm respectively at the two Q^2 values. To achieve the required precision, an event rate capability of up to 500 kHz was needed.

The main challenge of deep inelastic scattering experiments is the separation of scattered electrons from the pion background in the spectrometer and detector system. The neutral pions would decay into e^+e^- pairs, from which the electrons produced cannot be rejected by detectors and their effect on the measured asymmetry was analyzed in Ref. [3]. Charged pions are produced primarily from nucleon resonance decays and could carry a parity violation asymmetry corresponding to the Q^2 at which the resonances are produced, typically a fraction of the asymmetry of electrons with the same scattered momentum. Assuming a fraction $f_{\pi/e}$ of the detected events are π^- and $1 - f_{\pi/e}$ are electrons, the measured asymmetry is

$$A_m = f_{\pi/e} A_\pi + (1 - f_{\pi/e}) A_e, \tag{2}$$

where A_e is the desired electron scattering asymmetry and A_π is the asymmetry of the pion background. To extract A_e to a high precision, one needs to either minimize the pion contamination $f_{\pi/e}$ to a negligible level, or to correct the measured asymmetry for the asymmetry of pions, which itself needs to be measured precisely. For the PVDIS experiment, the goal was to control $f_{\pi/e}$ to the 10^{-4} level provided that the pion asymmetries do not exceed those of electrons.

The experiment used a 100 μA electron beam with a polarization of approximately 90% and a 20-cm long liquid deuterium target. The two High Resolution Spectrometers (HRS) [5] were used to detect scattered events. While the standard HRS detector package and data acquisition (DAQ) system routinely provide a 10^4 pion rejection with approximately 99% electron efficiency, they are based on full recording of the detector signals and are limited to event rates up to 4 kHz [5]. This is not sufficient for the high rates expected for the experiment. (The HRS DAQ will be referred to as "standard DAQ" hereafter.)

Recent parity violation electron scattering experiments, such as SAMPLE [6] at MIT-Bates, HAPPEX [7–11], and PREX [12] at JLab, focused on elastic scattering from nuclear or nucleon targets that are typically not contaminated by inelastic backgrounds. Signals from the detectors can be integrated and a helicity dependence in the integrated signal can be used to extract the physics asymmetry. An integrating DAQ was also used at the preceding PVDIS measurement at SLAC [13,14] in which approximately 2% of the integrated signal was attributed to pions. In the Mainz PVA4 experiment [15–17], particles were detected in a total absorption calorimeter and the integrated energy spectrum was recorded. Charged pions and other background were separated from electrons in the offline analysis

of the energy spectrum, and the pion rejection is in the order of 100:1 based on the characteristics of the calorimeter.

High performance particle identification can usually be realized in a counting-based DAQ where each event is evaluated individually. In the G0 experiment [18–22] at JLab, a superconducting spectrometer with a 2π azimuthal angle coverage was used to detect elastically scattered protons at the forward angle and elastic electrons at the backward angle. At the forward angle, protons were identified using time-of-flight. At the backward angle, pions were rejected from electrons using an aerogel Cherenkov counter and a pion rejection factor of $125:1$ or better was reported [22]. The deadtime correction of the counting system was at the order of a few percent [21,22].

While the PVDIS experiment could fully utilize existing spectrometers and detectors at JLab, upon examining all existing techniques for PV measurements it became clear that a custom electronics and DAQ were needed to control the systematic uncertainties due to data collection to below 1%. In this paper we describe a scaler-based, cost effective counting DAQ which limited the pion contamination of the data sample to a negligible level of $f_{\pi/e} \approx 10^{-4}$. Basic information of the detector package and the DAQ setup will be presented first, followed by the analysis on electron detection efficiency, pion rejection and contamination, corrections due to counting deadtime, and the statistical quality of the asymmetry measurement.

2 Detector and DAQ Overview

The design goal of the DAQ is to record data up to 1 MHz with hardware-based PID and well measured and understood deadtime effects. The following detectors in the HRS [5] were used to characterize scattered particles: Two scintillator planes provided the main trigger, while a CO_2 gas Cherenkov detector and a double-layer segmented lead-glass detector provided particle identification information. The vertical drift chambers (as the tracking detector) were used during calibration runs but were turned off during production data taking because they were not expected to endure the high event rates.

For the gas Cherenkov and the lead-glass detector, a full recording of their output ADC data is not feasible at the expected high rate. Instead their signals were passed through discriminators and logic units to form preliminary electron and pion triggers. Particle identification was fulfilled by the use of discriminators for both the lead-glass and the Cherenkov detectors and proper settings of their thresholds. These preliminary triggers were then combined with the scintillator triggers to form the final electron and pion triggers, which were sent to scalers to record the event counts and offline used to form asymmetries $A = (n_R - n_L)/(n_R + n_L)$, where $n_{R(L)}$ is the integrated rate of the triggers normalized to the integrated beam charge

for the right(R) and left(L) handed spin (helicity) states of the incident electron beam. The scalers that counted triggers and the beam charge were integrated over the helicity period, which was flipped pseudo-randomly at 30 Hz per the experimental technique used by the HAPPEX experiments [11].

For the HRS the two layers of the lead-glass detector are called "preshower" and "shower" detectors, respectively. The preshower blocks in the Right HRS (the spectrometer located to the right side of the beamline when viewed along the beam direction) has 48 blocks arranged in a 2×24 array, with the longest dimension of the blocks aligned perpendicular to the particle trajectory. For the two blocks in each row, only the ends facing outward are read out by photo-multiplier tubes (PMTs) and the other ends of the two blocks were facing each other and not read out. Therefore the preshower detector had 48 output channels. All preshower blocks were individually wrapped to prevent light leak. The shower detector in the Right HRS had 75 blocks arranged in a 5×15 array with the longest dimension of the blocks aligned along the trajectory of scattered particles. PMTs are attached to each block of the Right shower detector on one end only, giving 75 output channels. The preshower and the shower detectors in the Left HRS are similar to the preshower detector on the Right HRS except that for each detector there are 34 blocks arranged in a 2×17 array.

Because the lead-glass detectors in the Left and Right HRS are different, design of the lead-glass-based triggers of the DAQ is also different, as shown in Fig. 1. As a compromise between the amount of electronics needed and the rate in the front end logic modules, the lead-glass blocks in both the preshower and the shower detectors were divided into 6 (8) groups for the Left (Right) HRS, with each group consisting 8 blocks. On the Right HRS only 60 of the 75 shower blocks were used while the 15 blocks on the edge were not read out. The reduction on the HRS acceptance due to not using these side blocks is negligible. Signals from the 8 blocks in each group were added using a custom-made analog summing unit called the "SUM8 module", then passed to discriminators. The geometry and the position of each preshower group were carefully chosen to match those of the corresponding shower group to maximize electron detection efficiency. On the Left HRS adjacent groups in both preshower and shower had overlapping blocks, while for the Right HRS only preshower blocks were overlapping. To allow overlap between adjacent groups, signals from preshower blocks on the Right HRS and from both preshower and shower blocks on the Left HRS were split into two identical copies using passive splitters.

A schematic diagram of the DAQ electronics for the Right HRS is shown in Fig. 2. Preliminary electron and pion triggers were formed by passing shower (SS) and preshower (PS) signals and their sums, called total shower (TS) signals, through discriminators with different thresholds. For electron triggers, logical ANDs of the PS discriminator and the TS discriminator outputs were used. For pions, low threshold discriminators on the TS signal alone were sent to logical OR modules

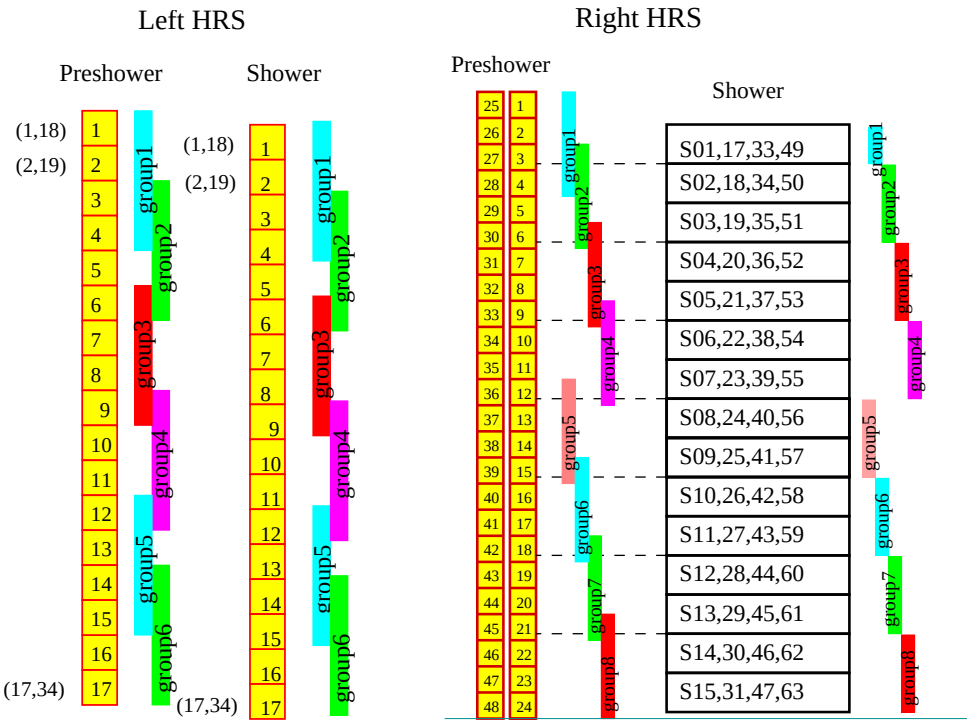

Fig. 1. [*Color online*] Grouping scheme (side-view) for the double-layer lead-glass detectors for the Left and the Right HRS. Scattered particles enter the detector from the left. The colored vertical bars represent the range of each group.

to produce preliminary triggers. Additional background rejection was provided by the "VETO" circuit, which combined signals from the gas Cherenkov (GC) and the "T1" signal [5] from scintillators (SC). Each valid coincidence between GC and T1 would produce an 150-ns wide electron VETO signal that allowed an output to be formed by the logical AND modules from the preliminary electron triggers. Each valid T1 signal without the GC signal would produce an 150-ns wide pion VETO signal that allowed an output to be formed by the logical OR modules from the preliminary pion triggers. The outputs of the logical AND and OR modules are called group electron and pion triggers, respectively. All six (eight) group electron or pion triggers were then ORed together to form the global electron or pion trigger for the Left (Right) HRS. All group and the final electron and pion triggers were counted using scalers. Because pions do not produce large enough lead-glass signals to trigger the high threshold TS discriminators for the electron triggers, pions do not introduce extra counting deadtime for the electron triggers. However, the 150-ns width of the electron VETO signal would cause pion contamination in the electron trigger. This effect will be presented in section 3.

In order to monitor the counting deadtime of the DAQ, two identical paths of electronics were constructed. The only difference between the two paths is in the PS and the TS discriminator output widths, set at 30 ns and 100 ns for the "narrow" and the "wide" paths, respectively. The scalers are rated for 250 MHz (4 ns deadtime) and therefore do not add to the deadtime. In addition, the output width of all

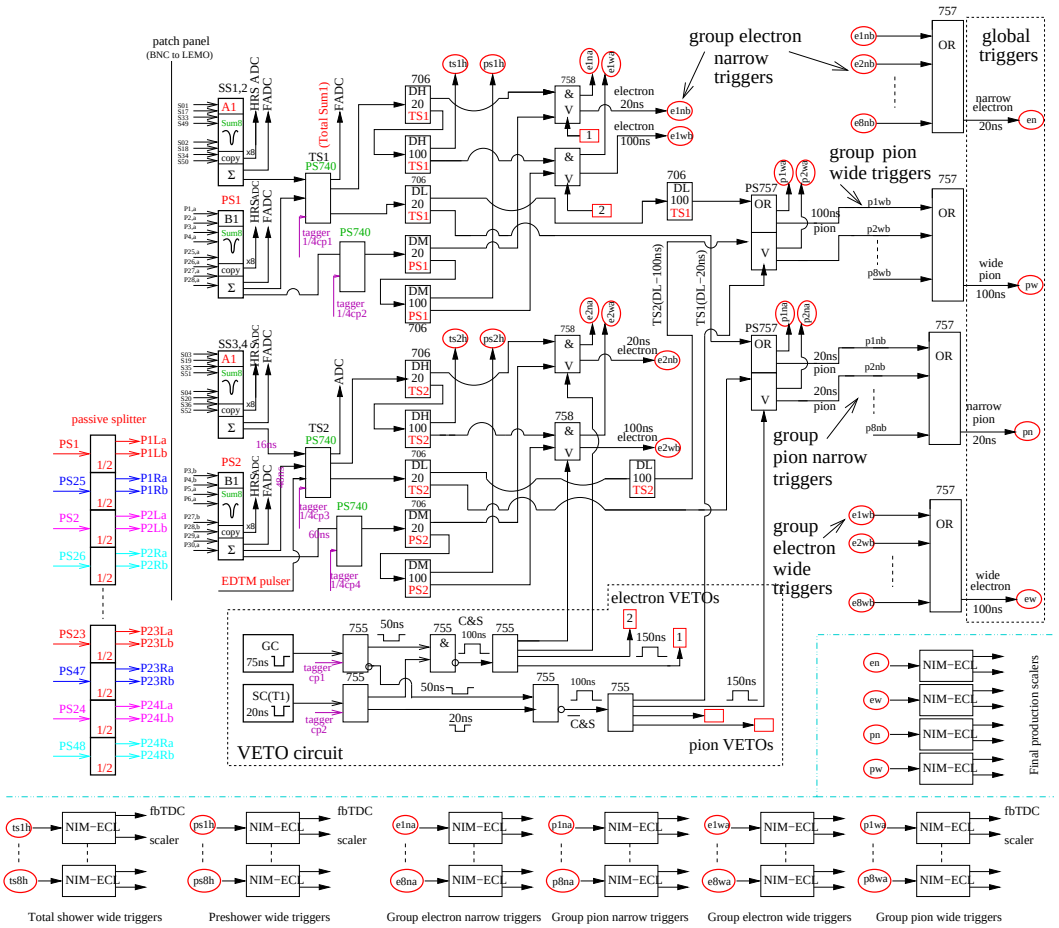

Fig. 2. [*Color online*] Electronics diagram for the Right HRS DAQ used by the PVDIS experiment. The Sum8's, discriminators and logic modules for two groups are shown, as well as the location of tagger signal inputs, setup of the VETO circuit using scintillator (SC) and gas Cherenkov (GC) signals, the logic units for combining triggers from all eight groups into final triggers, the counting scalers, and the monitoring fastbus TDCs. Electronics for the Left HRS are similar except for the grouping scheme.

logic modules were set to 15 ns, hence the deadtime of the DAQ for each group is dominated by the deadtime of the discriminators. Detailed analysis of the DAQ deadtime will be presented in section 4.

The SUM8 modules used for summing all lead-glass signals also served as fan-out modules, providing exact copies of the input PMT signals. These copies were sent to the standard HRS DAQ for calibration. During the experiment, data were collected at low rates using reduced beam currents with both DAQs functioning, such that a direct comparison of the two DAQs can be made. The vertical drift chambers were used during these low rate DAQ studies. Outputs from all discriminators, signals from the scintillator and the gas Cherenkov, and all electron and pion group and global triggers were sent to Fastbus TDCs (fbTDC) and were recorded in the standard DAQ. Data from these fbTDCs were used to align amplitude spectrum and timing of all signals. They also allowed the study of the Cherenkov and the

lead-glass detector performance for the new DAQ.

Full sampling of partial analog signals were done using Flash-ADCs (FADCs) at low rates intermittently during the experiment. For one group on the Left and one group on the Right HRS, the preshower and the shower SUM8 outputs, the intermediate logical signals of the DAQ, and the output electron and pion triggers were recorded. These FADC data provided a study of pileup effects to confirm the dead-time simulation and to provide the input parameters for the simulation, specifically the rise and fall times of the signals and their widths.

3 DAQ PID Performance

PID performance of the DAQ system was studied with calibration runs taken at low beam currents using fbTDC signals along with ADC data of all detector signals recorded by the standard DAQ. Events that triggered the DAQ would appears as a timing peak in the corresponding fbTDC spectrum of the standard DAQ and a cut on this peak can be used to select those events. Figure 3 shows the preshower vs. shower signals for group 2 on the Left HRS. A comparison between no fbTDC cut and with cut on the fbTDC signal of the electron wide trigger from this group clearly shows the hardware PID cuts.

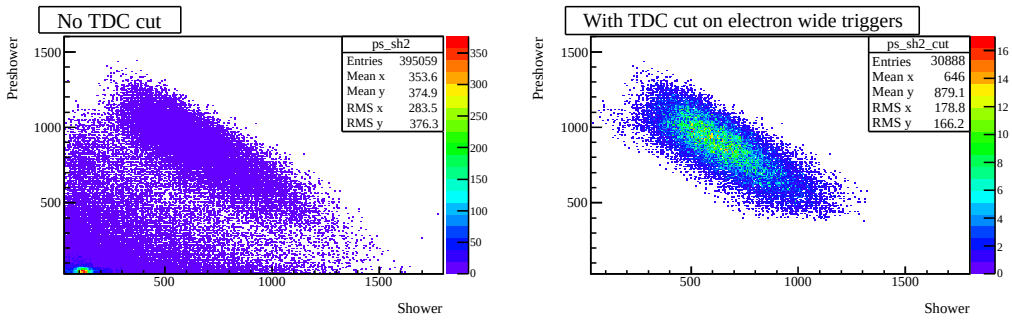

Fig. 3. [*Color online*] Preshower vs. Shower ADC data (sum of 8 blocks each) for group 2 on the Left HRS, without the fbTDC cut (left panel) and with cut on the group 2 electron wide trigger fbTDC signal (right panel). It clearly shows the thresholds on the preshower and the total shower signals, indicating the DAQ is selecting the correct events as electrons.

Electron efficiency and pion rejection factors of the lead-glass detector on the Left HRS during a one-hour run are shown in Fig. 4 as functions of the location of the hit of the particle in the preshower detector. PID performance on the Right HRS is similar. Electron efficiency from wide groups are slightly higher than narrow groups because there is less event loss due to timing mis-alignment when taking the coincidence between the preshower and the total shower discriminator outputs. Variations in the electron efficiency across the spectrometer acceptance effectively influence the Q^2 of the measurement. For this reason, low-rate calibration data

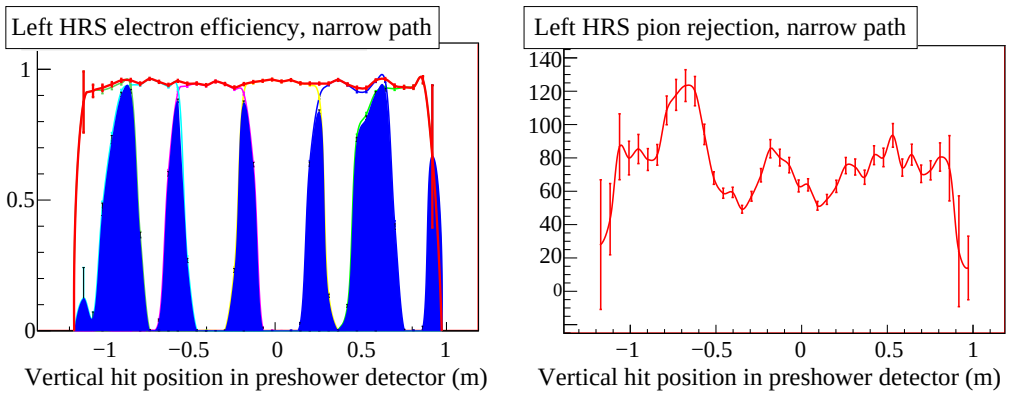

Fig. 4. [*Color online*] Electron detection efficiency (left) and pion rejection factor (right) vs. vertical (dispersive) hit position of the particle in the preshower detector for the narrow electron triggers in the Left HRS. A one-hour run with reduced beam current was used in this evaluation. For electron efficiencies, the total efficiency is shown by the red curve, while blue shaded area indicates events that were recorded by two adjacent groups. The average electron efficiency achieved by the lead glass detector alone for this one-hour run is $(94.626 \pm 0.002)\%$ and the average pion rejection factor is $(75.3 \pm 1.1) : 1$. The error bars are statistical only. PID performance for the wide path and the Right HRS are similar.

were taken daily during the experiment to monitor the DAQ PID performance and corrections were applied to the asymmetry data.

The gas Cherenkov detector signals were read out by 10 PMTs on both the Left and the Right HRS. Signals from all 10 PMTs were summed in an analog-sum module and sent to a discriminator. The discriminator output was sent to the DAQ (as shown in Fig. 2) as well as fbTDCs. Figure 5 shows the Cherenkov ADC sum with and without the fbTDC cut which clearly shows the capability of rejecting pions.

As described in the Introduction, pion contamination in the electron trigger would affect the measured electron asymmetry as $A_m = (1 - f_{\pi/e})A_e + f_{\pi/e}A_\pi$ where A_m and A_e are the measured and the true electron asymmetries, respectively, and A_π is the parity violation asymmetry of pion production. The pion contamination in the electron trigger, $f_{\pi/e}$, comes from two effects: There is a small possibility that a pion could trigger both the lead-glass and the gas Cherenkov detectors, causing a false electron trigger output. This possibility is determined by the direct combination of the pion rejection factors of the two detectors and is below 10^{-4}. A larger effect comes from the width of the electron VETO signal: Since each coincidence between the gas Cherenkov and the scintillator signals would open the electron counting gate (electron VETO) by 150 ns, while the DAQ deadtime of the lead-glass detector is less than this value, pions that arrived after the DAQ deadtime but before the closing of the electron VETO signal would cause a false electron trigger. The sum of the two effects can be written as

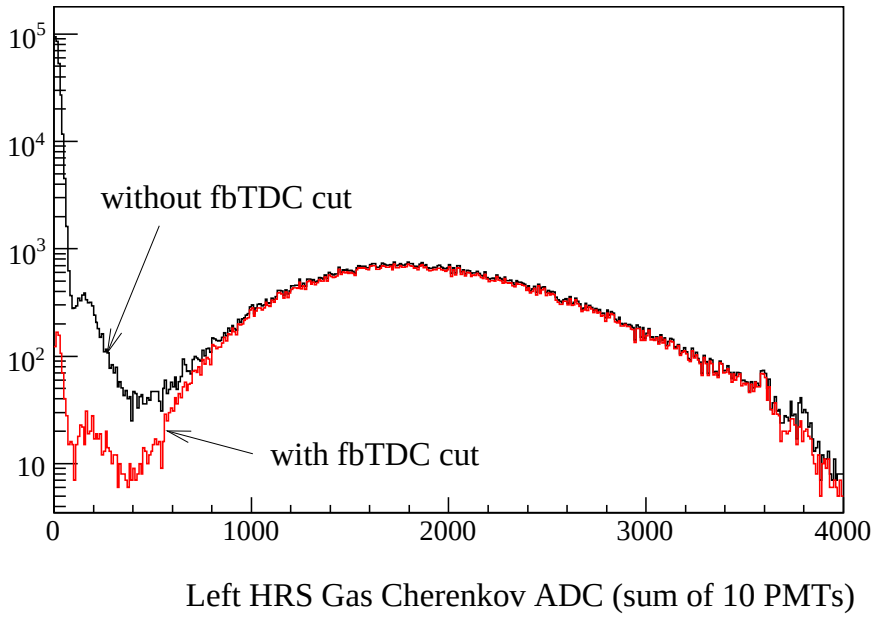

Fig. 5. [*Color online*] Gas Cherenkov ADC data (sum of 10 PMTs) for the Left HRS during a one-hour run at $Q^2 = 1.9$ (GeV/c)^2, with a fbTDC cut on the Cherenkov discriminator output (red) and without (black). The beam current during this run was about 100 μA, the incident electron rate on the detector was about 23 kHz with a pion to electron rate ratio of approximately 3.5. The discriminator clearly selected electrons while rejecting pions.

$$f_{\pi/e,n(w)} = \frac{R_\pi \eta_\pi^{GC} \eta_\pi^{LG}}{R_e \eta_e^{GC} \eta_e^{LG}} + \frac{R_\pi \eta^{LG} \left\{ R_e \eta_e^{GC} \left[150 \text{ ns} - \tau_{n(w)} \right] \right\}}{R_e \eta_e^{GC} \eta_e^{LG}}$$

where R_e and R_π are the input electron and the pion rates, respectively; $\eta_e^{LG(GC)}$ is the electron detection efficiency of the lead-glass (gas Cherenkov) detectors, and $\eta_\pi^{LG(GC)}$ is the pion detection efficiency, i.e., the inverse of the rejection factor, of the lead-glass (gas Cherenkov) detector. The DAQ group deadtime of the lead-glass detector for the narrow (wide) path, $\tau_{n(w)}$, is approximately 60 ns (100-110 ns) and the analysis obtaining these results will be presented in the next section. The term $R_e \eta_e^{GC} \left[150 \text{ ns} - \tau_{n(w)} \right]$ gives the probability for a pion to arrive within a valid electron VETO signal and thus can not be rejected by the lead-glass detectors.

The electron detection efficiency and pion rejection factor averaged throughout the experiment are shown in table 1 for different kinematics and for the Left and the Right HRS separately. Also shown are the π/e rate ratio obtained from the data and the resulting pion contamination $f_{\pi/e}$ evaluated separately for the narrow and the wide paths.

As shown in table 1, the overall pion contamination was at the order of 2×10^{-4} or lower. Because pions are produced from nucleon resonance decays, the parity violation asymmetry of pion production is expected to be no larger than that of

Table 1
Average electron detection efficiency and pion rejection factor achieved through the lead glass (LG) and the gas Cherenkov (GC) detectors, respectively, and the combined performance. The error bars of the efficiencies and the rejection factors are statistical only. The error bars for $f_{\pi/e}$ are shown separately for statistical uncertainties, systematic uncertainties due to our understanding of the rates, detector efficiencies and deadtimes, and systematic uncertainties due to day-to-day variations since calibration runs were taken only once a day.

Kinematics and Spectrometer combinations			
	$Q^2 = 1.1$ (GeV/c)^2	$Q^2 = 1.9$ (GeV/c)^2	
HRS	Left	Left	Right
Electron detection efficiency η_e			
GC	$(99.14 \pm 0.02)\%$	$(99.03 \pm 0.03)\%$	$(98.19 \pm 0.06)\%$
LG, narrow	$(91.93 \pm 0.04)\%$	$(94.50 \pm 0.06)\%$	$(94.36 \pm 0.04)\%$
LG, wide	$(92.88 \pm 0.04)\%$	$(95.79 \pm 0.06)\%$	$(95.23 \pm 0.04)\%$
combined, narrow	$(91.14 \pm 0.04)\%$	$(93.58 \pm 0.06)\%$	$(92.65 \pm 0.07)\%$
combined, wide	$(92.08 \pm 0.04)\%$	$(94.86 \pm 0.06)\%$	$(93.51 \pm 0.07)\%$
Pion rejection $1/\eta_\pi$			
GC	$(158.6 \pm 3.5) : 1$	$(301.2 \pm 5.2) : 1$	$(414.3 \pm 6.2) : 1$
LG, narrow	$(101.5 \pm 1.6) : 1$	$(78.9 \pm 0.9) : 1$	$(72.7 \pm 0.3) : 1$
LG, wide	$(103.9 \pm 1.7) : 1$	$(81.5 \pm 1.0) : 1$	$(74.3 \pm 0.3) : 1$
Pion contamination in the electron trigger $f_{\pi/e}$, narrow path			
actual rate R_π/R_e	0.7	3.5	3.5
$f_{\pi/e,n}$	1.61×10^{-4}	2.20×10^{-4}	1.99×10^{-4}
$\Delta f_{\pi/e,n}$(stat.)	$\pm 3.34 \times 10^{-6}$	$\pm 4.62 \times 10^{-6}$	$\pm 2.15 \times 10^{-6}$
$\Delta f_{\pi/e,n}$(syst.)	$\pm 2.01 \times 10^{-5}$	$\pm 2.29 \times 10^{-5}$	$\pm 2.08 \times 10^{-5}$
$\Delta f_{\pi/e,n}$(var.)	$\pm 9.76 \times 10^{-6}$	$\pm 1.71 \times 10^{-5}$	$\pm 1.15 \times 10^{-5}$
$\Delta f_{\pi/e,n}$(total)	$\pm 2.24 \times 10^{-5}$	$\pm 2.86 \times 10^{-5}$	$\pm 2.38 \times 10^{-5}$
Pion contamination in the electron trigger $f_{\pi/e}$, wide path			
$f_{\pi/e,w}$	1.00×10^{-4}	1.83×10^{-4}	1.59×10^{-4}
$\Delta f_{\pi/e,w}$(stat.)	$\pm 2.28 \times 10^{-6}$	$\pm 4.27 \times 10^{-6}$	$\pm 2.10 \times 10^{-6}$
$\Delta f_{\pi/e,w}$(syst.)	$\pm 1.71 \times 10^{-5}$	$\pm 2.01 \times 10^{-5}$	$\pm 1.96 \times 10^{-5}$
$\Delta f_{\pi/e,w}$(var.)	$\pm 9.81 \times 10^{-6}$	$\pm 1.51 \times 10^{-5}$	$\pm 1.02 \times 10^{-5}$
$\Delta f_{\pi/e,w}$(total)	$\pm 1.97 \times 10^{-5}$	$\pm 2.52 \times 10^{-5}$	$\pm 2.21 \times 10^{-5}$

scattered electrons with the same momentum. This was confirmed by asymmetries formed from pion triggers during this experiment. The uncertainty in the electron asymmetry due to pion contamination is therefore at the order of 2×10^{-4} and is negligible compared to the $3 - 4\%$ statistical uncertainty.

To understand fully the effect of pion background on the measured electron asymmetry, it is important to extract asymmetries of the pion background to confirm that they are indeed smaller than the electron asymmetry. A complete PID analysis was carried out on the pion triggers of the DAQ where the electron contamination in the pion trigger $f_{e/\pi}$ was evaluated in a similar method as $f_{\pi/e}$ above, following

$$f_{e/\pi,n(w)} = \frac{R_e \xi_e^{GC} \xi_e^{LG}}{R_\pi \xi_\pi^{GC} \xi_\pi^{LG}} + \frac{R_e \xi^{LG} \left\{ R_\pi \xi_\pi^{GC} \left[150 \text{ ns} - \tau_{n(w)} \right] \right\}}{R_\pi \xi_\pi^{GC} \xi_\pi^{LG}}$$

where as before R_e and R_π are the electron and the pion rates incident on the detectors, respectively; The detection efficiencies ξ are now defined for the pion triggers of the DAQ: $\xi_e^{LG(GC)}$ is the electron detection efficiency of the lead-glass (gas Cherenkov) detectors, and $\xi_\pi^{LG(GC)}$ is the pion detection efficiency of the lead-glass (gas Cherenkov) detector in the pion triggers. Although the goal of the pion triggers is to collect pions, only the gas Cherenkov played a role in rejecting electrons in the pion trigger, and all electrons would form valid pion triggers in the lead-glass counters. Therefore $\xi_e^{LG} \approx 1$ and the electron contamination is high. Results for electron contamination in the pion trigger is summarized in Table 2.

4 DAQ Deadtime

Deadtime is the amount of time after an event during which the system is unable to record another event. Identifying the exact value of the deadtime is always a challenge in counting experiments. By having a narrow and a wide path, we can observe the trend in the deadtime – the wider path should have higher deadtime. By matching the observed trend with our simulation we can benchmark and confirm the result of our deadtime simulation. In addition, dividing lead-glass blocks into groups greatly reduces the deadtime loss in each group compared to summing all blocks together and forming only one final trigger.

To illustrate the importance of the deadtime, consider its effect on the asymmetry A. For a simple system with only one contribution to the deadtime loss δ, the observed asymmetry A_O is related the the true asymmetry A according to $A_O = (1 - \delta)A$. In this experiment δ was expected to be on the order of (1-2)%. Since the statistical accuracy on the asymmetry is (3-4)%, it was desired to know δ with a (10-20)% relative accuracy so that it would become a negligible systematic error. The DAQ used in this experiment, however, was more complex and had three contributions to the deadtime as listed below:

Table 2
Average pion detection efficiency and electron rejection factor achieved through the lead glass (LG) and the gas Cherenkov (GC) detectors, respectively, and the combined performance. The error bars of the efficiencies and the rejection factors are statistical only. The error bars for $f_{e/\pi}$ are shown separately for statistical uncertainties, systematic uncertainties, and the systematic uncertainty due to day-to-day variations since calibration runs were taken only on a daily basis.

Kinematics and Spectrometer Combinations			
	$Q^2 = 1.1$ (GeV/c)^2	$Q^2 = 1.9$ (GeV/c)^2	
HRS	Left	Left	Right
Pion detection efficiency η_π			
GC	$(99.52 \pm 0.01)\%$	$(99.73 \pm 0.01)\%$	$(99.74 \pm 0.01)\%$
LG, narrow	$(21.67 \pm 0.01)\%$	$(79.72 \pm 0.02)\%$	$(15.61 \pm 0.01)\%$
LG, wide	$(21.67 \pm 0.01)\%$	$(79.71 \pm 0.02)\%$	$(15.60 \pm 0.01)\%$
combined, narrow	$(21.57 \pm 0.01)\%$	$(79.70 \pm 0.02)\%$	$(15.57 \pm 0.01)\%$
combined, wide	$(21.57 \pm 0.01)\%$	$(79.69 \pm 0.02)\%$	$(15.56 \pm 0.01)\%$
Electron rejection $1/\eta_e$			
GC	$(31.42 \pm 0.78) : 1$	$(89.44 \pm 2.48) : 1$	$(48.48 \pm 1.55) : 1$
LG, narrow	$(1.0468 \pm 0.0003) : 1$	$(1.0487 \pm 0.0005) : 1$	$(1.0271 \pm 0.0002) : 1$
LG, wide	$(1.0469 \pm 0.0003) : 1$	$(1.0499 \pm 0.0005) : 1$	$(1.0279 \pm 0.0002) : 1$
Electron contamination in pion triggers $f_{e/\pi}$, narrow path			
actual rate R_π/R_e	0.7	3.5	3.5
$f_{e/\pi,n}$	0.2738	0.03197	0.00967
$\Delta f_{e/\pi,n}$(stat.)	± 0.00386	± 0.00080	0.00026
$\Delta f_{e/\pi,n}$(syst.)	± 0.01382	± 0.00143	0.00026
$\Delta f_{e/\pi,n}$(var.)	± 0.05441	± 0.00303	0.00112
$\Delta f_{e/\pi,n}$(total)	± 0.05613	± 0.00335	0.00115
Electron contamination in pion triggers $f_{e/\pi}$, wide path			
$f_{e/\pi,w}$	0.2246	0.02672	0.00854
$\Delta f_{e/\pi,w}$(stat.)	± 0.00386	± 0.00079	0.00026
$\Delta f_{e/\pi,w}$(syst.)	± 0.01236	± 0.00127	0.00062
$\Delta f_{e/\pi,w}$(var.)	± 0.05255	± 0.00308	0.00109
$\Delta f_{e/\pi,w}$(total)	± 0.05399	± 0.00333	0.00125

(1) The “group” deadtime: deadtime due to discriminators and logical AND modules used to form group triggers;
(2) The “veto” deadtime: deadtime from the VETO circuit that used scintillators and gas Cherenkov signals to form the “gate” signals, which controlled the AND (OR) module of each group to form group electron (pion) triggers.
(3) The “OR” deadtime: deadtime due to the logical OR module used to combine all group triggers into final global triggers.

The total deadtime is a combination of all three. In order to evaluate the DAQ deadtime, a full-scale trigger simulation is necessary. This trigger simulation will be described in the next section followed by results on the group, veto, and OR deadtime as well as on the total deadtime correction that was applied to the asymmetry data.

4.1 Trigger Simulation

The Hall A Trigger Simulation (HATS) was developed for the purpose of deadtime study for this experiment. The inputs to HATS include the analog signals for preshower, shower, scintillator and gas Cherenkov. The signal amplitudes were provided by ADC data from low-current runs and the signal rates were from high-current production runs. The rise and fall times for the preshower and shower SUM8 outputs play an important role in HATS. The signal shape is simulated with the function $S(t) = Ate^{-t/\tau}$, where A is related to the amplitude of the signal and the time constant τ was detemined from FADC data, see Fig. 6.

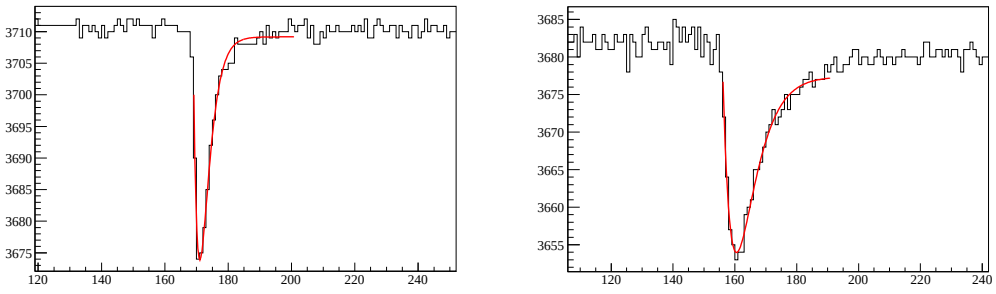

Fig. 6. [*Color online*] Calibration of time constans τ for Preshower (left) and Shower (right) of the Right HRS. The FADC snapshot (black) is compared with the fit $S(t) = Ate^{-t/\tau}$ (red).

With the recorded DAQ electronics and delay cables, HATS first rebuilds the DAQ system on the software level.At each nano-second, detector input signals are generated randomly according to the actual event rates and signal shape, and HATS simulates output signals from all discriminators, AND, and OR modules. Figure 7 shows a fraction of the DAQ electronics and the simulated results for a very short time period. By comparing output to input signals, HATS provides results on the

fractional loss due to deadtime for all group and global triggers w.r.t. the input signal.

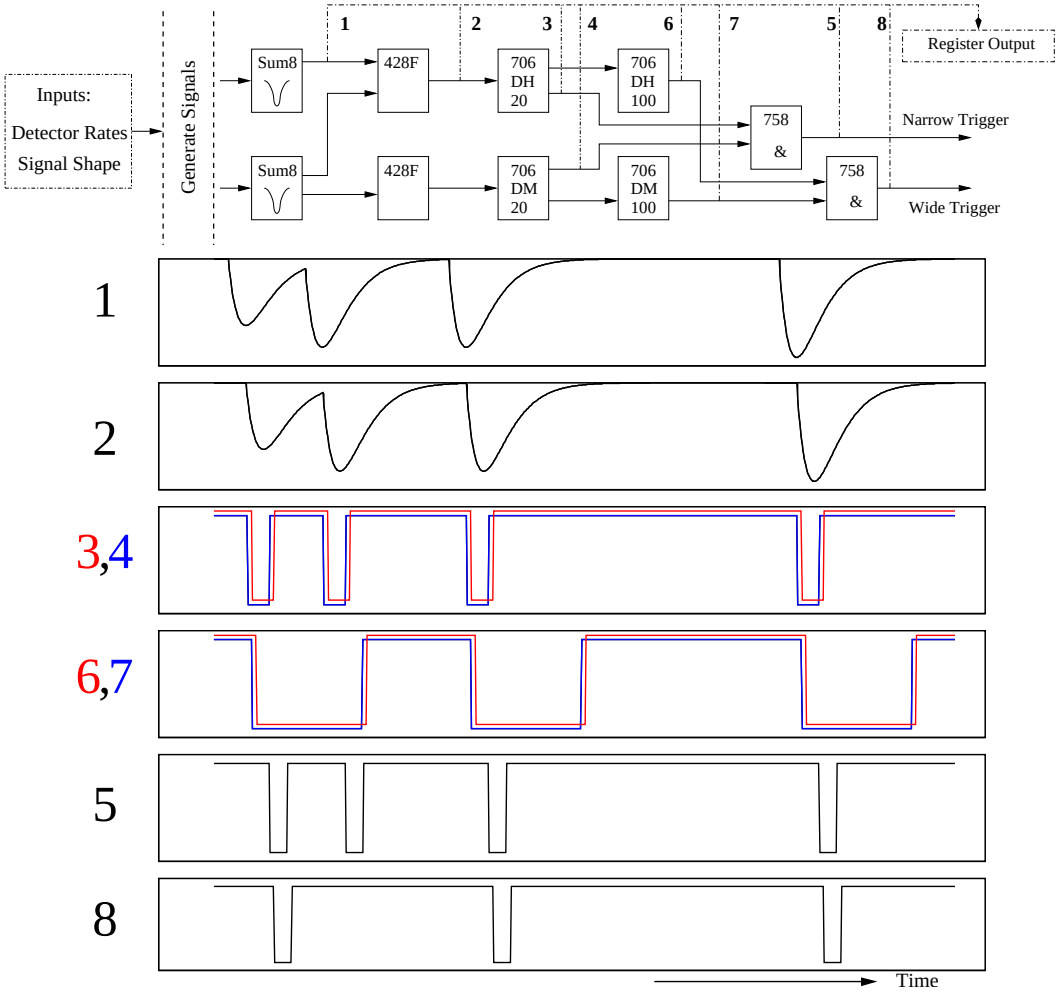

Fig. 7. [*Color online*] Top: A fraction of the group electron trigger. Each point corresponds to: 1 – Shower sum of the group; 2 – Total shower sum of the group; 3 – Total shower discriminator output (high threshold), narrow path; 4 – Preshower discriminator output (medium threshold), narrow path; 5 – group electron trigger, narrow path; 6 – Total shower discriminator output, wide path; 7 – Preshower discriminator output, wide path; 8 – group electron trigger, wide path. Bottom: Signals 1-8 as simulated by HATS. One can see that the second physical event is recorded by the narrow path group trigger (5) but not the wide path (8) due to deadtime loss.

4.2 Group Deadtime Measurement

In order to study the group deadtime, a high rate pulser signal ("tagger") was mixed with the Cherenkov and all preshower and total shower signals using analog summing modules, see Figs. 2 and 8. In the absence of all detector signals, a tagger pulse produces without loss an electron trigger output, and a "tagger-trigger coin-

cidence" pulse between this output and the "delayed tagger" – the tagger itself with an appropriate delay to account for the DAQ response time. When high-rate detector signals are present, however, some of the tagger pulses would not be able to trigger the DAQ due to deadtime. The deadtime loss in the electron trigger output w.r.t. the tagger input has two components:

(1) The count loss R_o/R_i: when a detector PMT signal precedes the tagger signal by a time interval δt shorter than the DAQ deadtime but longer than $w+t_1$, the tagger signal is lost and no coincidence output is formed. Here w is the width of the electron trigger output and t_1 is the time interval the delayed tagger precedes the tagger's own trigger output, see Fig. 8. During the experiment w was set to 15 ns for all groups, t_1 was measured at the end of the experiment and was found to be between 20 and 40 ns for all narrow and wide groups of the two HRSs.

(2) The pileup fraction p: when a PMT signal precedes the tagger signal by a time interval δt shorter than $w+t_1$, there would be coincidence output between the delayed tagger and the electron output triggered by the detector PMT signal. If furthermore δt is less than the DAQ deadtime (which is possible for this experiment since the deadtime is expected to be as long as 100 ns for the wide path), the tagger itself is lost due to deadtime and the tagger-trigger coincidence is a false count and should be subtracted. In the case if δt is shorter than $w + t_1$ but longer than the DAQ deadtime (not possible for this experiment but could happen in general), the tagger itself also triggers a tagger-trigger coincidence but in this case, there are two tagger-trigger coincidence events, both are recorded by the fbTDC if working in the multi-hit mode, and one is a false count and should be subtracted.

    The pileup effect can be measured using the delay between the tagger-trigger coincidence output and the input tagger. This is illustrated in Fig. 8 and the pileup effect contributes to both I_1 and I_2 regions of the fbTDC spectrum. Fractions of I_1 and I_2 relative to I_0 are expected to be $I_1/I_0 = Rt_1$ and $I_2/I_0 = Rw$, respectively, where R is the PMT signal rate. The pileup effect was measured using fbTDC spectrum for electron narrow and wide triggers for all groups. Data for $I_{1,2}$ extracted from fbTDC agree very well with the expected values.

The relative loss of tagger events due to DAQ deadtime is evaluated as

$$D = 1 - (1 - p)(R_o/R_i), \tag{3}$$

where R_i is the input tagger rate, R_o is the output tagger-trigger coincidence rate, and $p = (I_1 + I_2)/I_0$ is a correction factor for pileup effects as defined in Fig. 8. Results for the deadtime loss D are shown in Figs. 9 and 10, for group 4 on the left HRS and group 4 on the right HRS, respectively, and are compared with simulation. Different beam currents between 20 and 100 μA were used in this dedicated deadtime measurement. In order to reduce the statistical fluctuation caused by limited

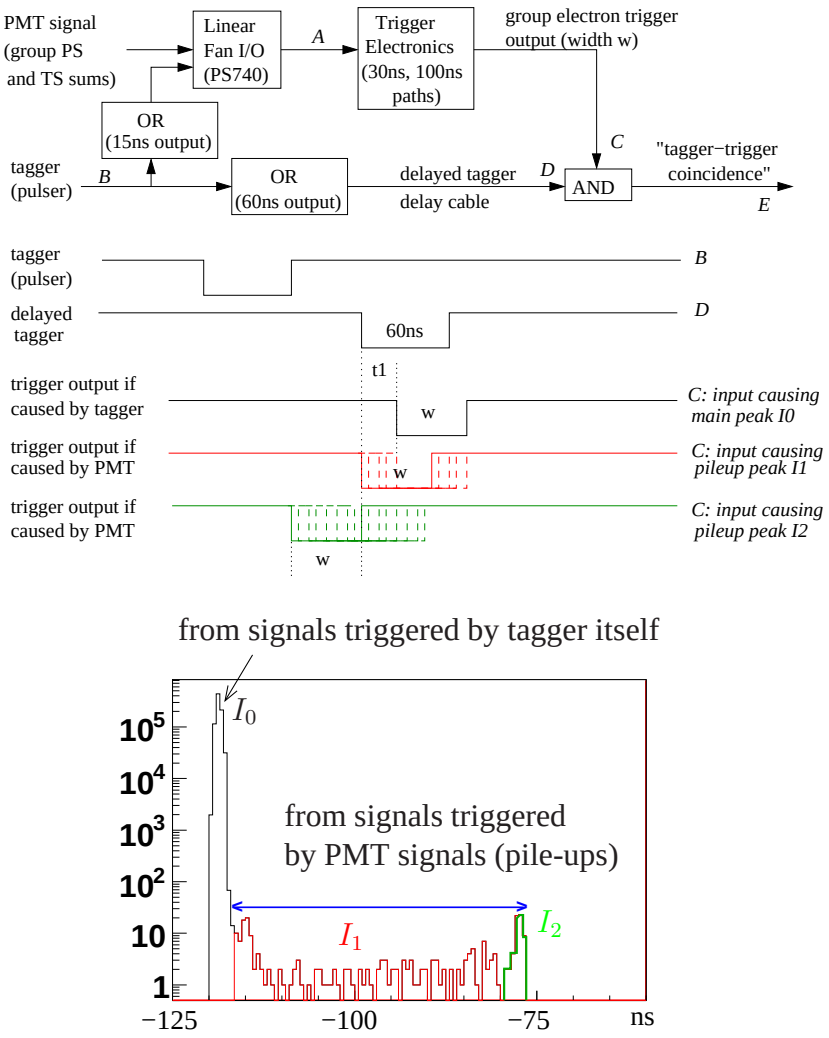

Fig. 8. [*Color online*] Top: schematic diagram for the tagger setup and signal timing sequence. The two logical OR units immediately following the tagger input "*B*" serve as width adjusters. Bottom: fbTDC spectrum for the relative timing between tagger-trigger coincidence and the input tagger, in 0.5-ns bins. The fbTDC module worked in a common stop and the multi-hit mode. Two different scenarios are shown: 1) Main peak I_0: when there is no PMT signal preceding the tagger, the tagger triggers the DAQ and forms a tagger-trigger coincidence. 2) Pileup events I_1 and I_2: when there is a PMT signal preceding the tagger by a time interval shorter than $w + t_1$, the PMT signal triggers the DAQ and forms a tagger-trigger coincidence signal with the delayed tagger.

number of trials in the simulation within a realistic computing time, simulations were done at higher rates than the actual measurement.

The slope of the tagger loss vs. event rate, as shown in Figs. 9 and 10, gives the value of group deadtime in seconds. One can see that the deadtime for the wide path is approximately 100 ns as expected. The deadtime for the narrow path, on the other hand, is dominated by the input PMT signal width (typically 60-80 ns)

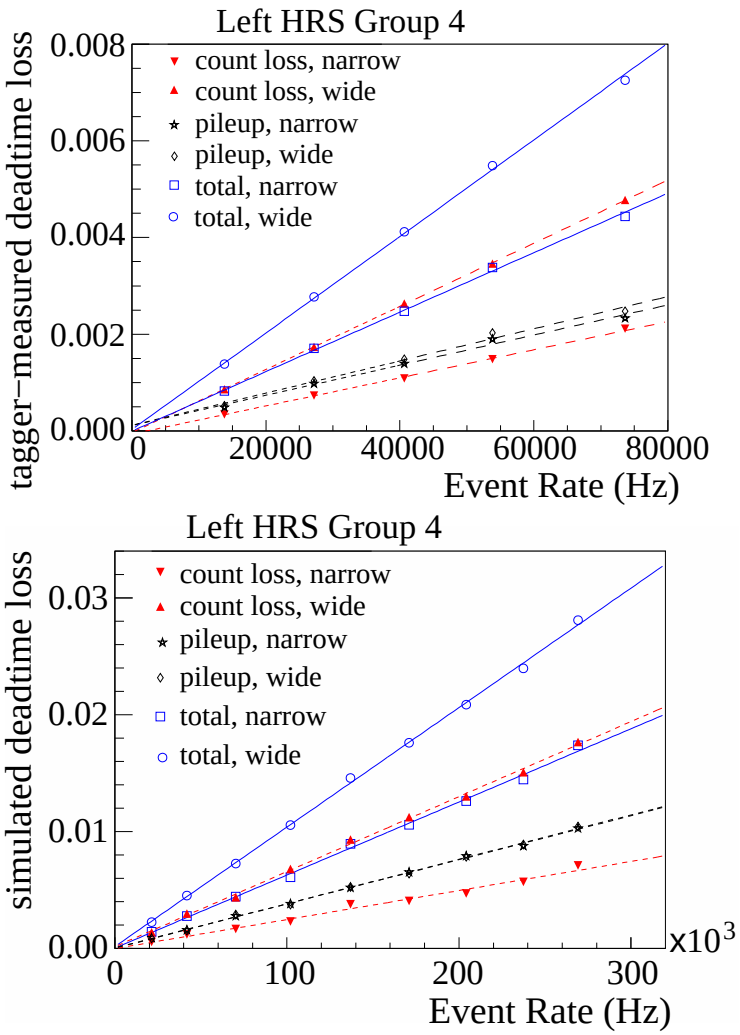

Fig. 9. [*Color online*] Deadtime loss in percent vs. event rate from the tagger method for group 4 on the Left HRS. Top: actual deadtime loss from tagger measurements; Bottom: simulated deadtime loss of the tagger. The tagger fractional count loss $1 - R_o/R_i$ (red) and the pileup correction p (black) are combined to form the total group deadtime D (blue). These data were taken (or simulated) at a Q^2 of 1.1 (GeV/c)^2. To minimize the statistical uncertainty while keeping the computing time reasonable, the simulation used higher event rates than the tagger measurement. The total group deadtime can be determined from the linear fit slope coefficients: tagger data narrow $p_1 = (61.5 \pm 0.2) \times 10^{-9}$ s, wide $p_1 = (99.9 \pm 0.3) \times 10^{-9}$ s, simulation narrow $p_1 = (62.5 \pm 1.4) \times 10^{-9}$ s, wide $p_1 = (102 \pm 1.3) \times 10^{-9}$ s. Group 4 is from the central blocks of the lead-glass detector and has the highest rate among all groups.

386 instead of the 30-ns discriminator width. The simulated group deadtime agree with
387 the data at a 10% level or better, for both HRSs and for both wide and narrow paths.

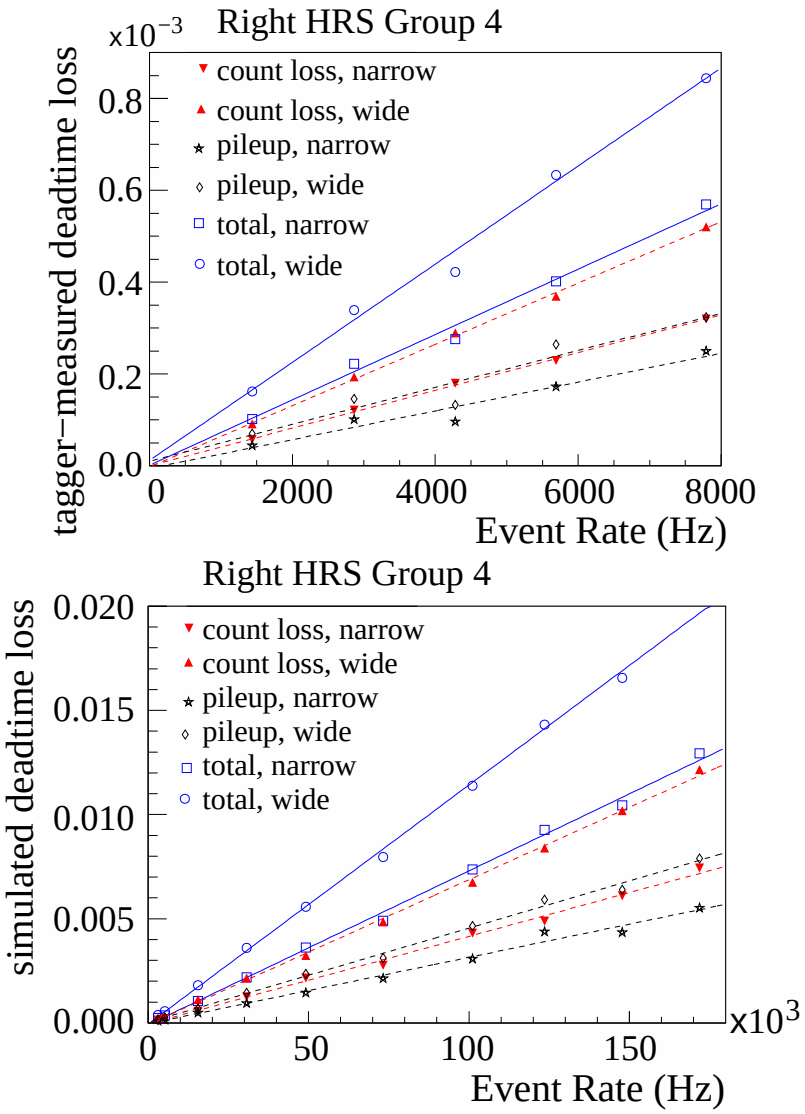

Fig. 10. [*Color online*] Deadtime loss in percent vs. group event rate from the tagger method for group 4 on the Right HRS. Top: tagger data; Bottom: simulation. These data were taken (or simulated) at a Q^2 of 1.9 (GeV/c)^2. The total group deadtime can be determined from the linear fit slope coefficient p_1: tagger data narrow $p_1 = (71.1 \pm 0.9) \times 10^{-9}$ s, wide $p_1 = (107 \pm 1.2) \times 10^{-9}$ s, simulation narrow $p_1 = (73.9 \pm 1.5) \times 10^{-9}$ s, wide $p_1 = (115 \pm 1.5) \times 10^{-9}$ s. Group 4 is from the central blocks of the lead-glass detector and has the highest rate among all groups. See Fig. 9 caption for details.

4.3 Total Deadtime Evaluation

Although the deadtime loss of each group was measured using tagger signals, the dominating term in the total deadtime is from the veto electronics because the trigger rate from scintillators and the gas Cherenkov is much higher than the individual lead-glass group rates. The difference in total loss between narrow and wide path is thus smaller than that in their group deadtimes. Simulation for the veto dead-

time was compared with FADC data and the agreement was found to be at 20% level or better. After subtracting group and veto deadtimes from the total simulated deadtime, the remaining is attributed to the logical OR module. There is no direct measurement of the logical OR deadtime, but the effect of the logical OR module is quite straightforward and can be calculated analytically. The difference between the simulation and the analytic results was used to estimate the uncertainty of the OR deadtime.

The simulated deadtime loss of the global electron triggers and its decomposition into group, veto, and OR are shown in Table 3. The deadtime loss is also shown in Fig. 11 as a function of the total event rate. The deadtime corrections at an 100 μA

Table 3
Simulated DAQ deadtime loss in percent for all kinematics and for both narrow (n) and wide (w) paths, along with the fractional contributions from group, veto, and OR deadtimes. The fractional deadtime from OR is calculated as one minus those from group and veto, and its uncertainty is estimated from the difference between simulation and the analytical results. The uncertainty of the total deadtime is the uncertainties from group, veto and OR added in quadrature.

HRS, Q^2	Path	fractional contribution			Total deadtime
(GeV/c)^2		Group	Veto	OR	loss at 100μA
Left, 1.1	n	$(20.6 \pm 2.1)\%$	$(51.3 \pm 4.5)\%$	$(28.1 \pm 4.7)\%$	$(1.45 \pm 0.10)\%$
	w	$(29.5 \pm 2.4)\%$	$(45.3 \pm 4.0)\%$	$(25.3 \pm 4.6)\%$	$(1.64 \pm 0.11)\%$
Left, 1.9	n	$(5.42 \pm 0.8)\%$	$(81.1 \pm 7.1)\%$	$(13.5 \pm 7.0)\%$	$(0.50 \pm 0.05)\%$
	w	$(8.39 \pm 0.4)\%$	$(77.3 \pm 6.8)\%$	$(14.3 \pm 8.0)\%$	$(0.52 \pm 0.06)\%$
Right, 1.9	n	$(2.9 \pm 0.2)\%$	$(80.6 \pm 18.5)\%$	$(16.5 \pm 12.7)\%$	$(0.89 \pm 0.20)\%$
	w	$(4.3 \pm 0.4)\%$	$(76.6 \pm 17.5)\%$	$(19.1 \pm 15.5)\%$	$(0.93 \pm 0.22)\%$

beam current for the narrow path triggers are $(1.45 \pm 0.13)\%$ and $(0.89 \pm 0.20)\%$, and for the wide path triggers are $(1.64 \pm 0.16)\%$ and $(0.93 \pm 0.22)\%$, for $Q^2 = 1.1$ and 1.9 (GeV/c)^2, respectively. These provide a direct correction to the measured asymmetry and the uncertainties are small compared to other dominant systematic uncertainties such as the beam polarization measurement. In practice, the deadtime correction is applied to data on a run by run basis with the deadtime of each run calculated using the actual beam current during the run and the linear fitting results from Fig. 11.

4.4 Asymmetry Measurement

The physics asymmetries sought for in this experiment were expected to be 91 and 160 ppm, for $Q^2 = 1.1$ and 1.9 (GeV/c)^2, respectively. The measured asymmetries

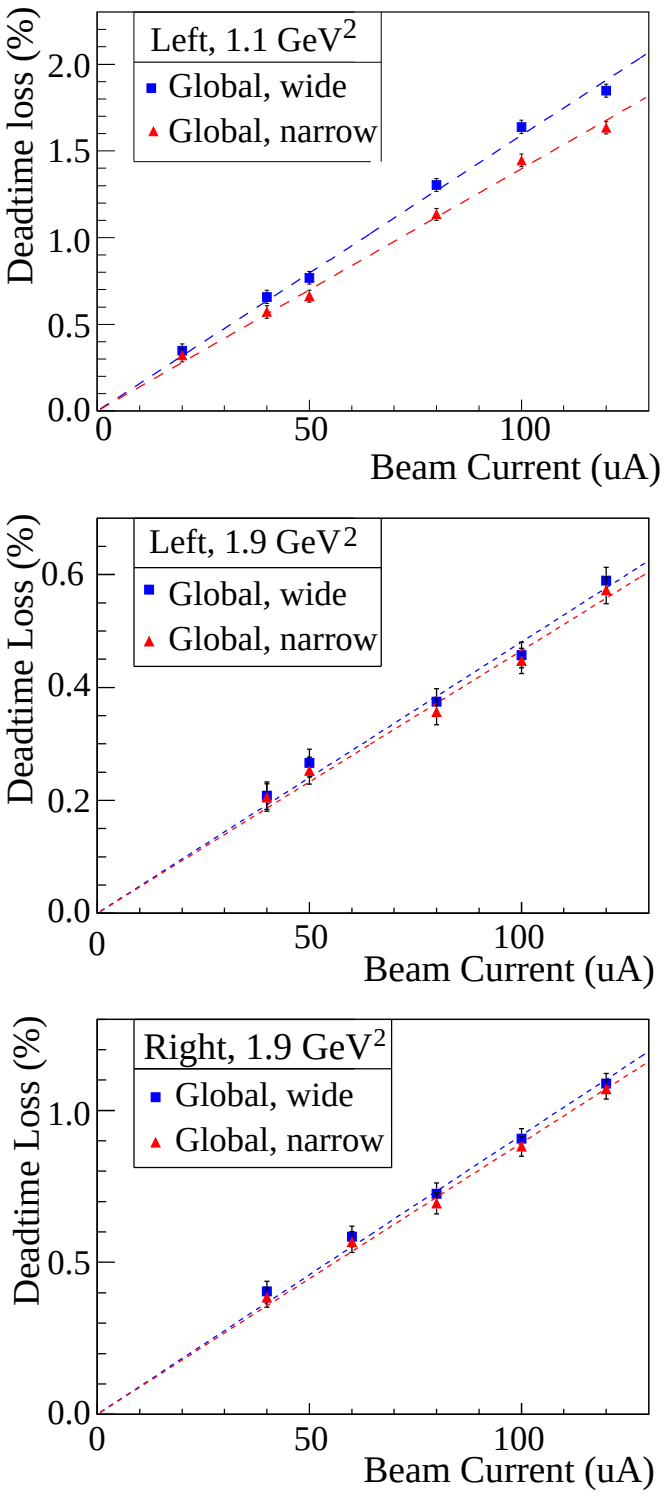

Fig. 11. [*Color online*] Simulated deadtime loss of the global electron trigger for the Left HRS at $Q^2 = 1.1$ (GeV/c)^2 (top), the Left HRS at $Q^2 = 1.9$ (GeV/c)^2 (middle), and the Right HRS at $Q^2 = 1.9$ (GeV/c)^2 (bottom). The error bars shown are due to statistical uncertainty of the simulation. See Table 3 for final uncertainty evaluation.

were about 90% of these values due to beam polarization. To understand the systematics of the asymmetry measurement, a half-wave plate (HWP) was inserted in the beamline to flip the laser helicity in the polarized source during half of the data taking period. The measured asymmetries flipped sign for each beam HWP change and the magnitude of the asymmetry remained consistent within statistical error bars.

The asymmetries can be formed from event counts of each beam helicity pair, with 33-ms of helicity right and 33-ms of helicity left beam, normalized by the beam charge. Figure 12 shows the pull distribution of these pair-wise asymmetries with the "pull" defined as

$$p_i \equiv (A_i - \langle A \rangle)/\delta A_i \ , \tag{4}$$

where A_i is the asymmetry extracted from the i-th beam helicity pair with the HWP states already corrected and $\delta A_i = 1/\sqrt{N_i^R + N_i^L}$ its statistical uncertainty with $N_i^{R(L)}$ the event count from the right (left) helicity pulse of the pair, and $\langle A \rangle$ is the asymmetry averaged over all beam pairs. One can see that the asymmetry spectrum agrees to five orders of magnitude with the Gaussian distribution, as expected from purely statistical fluctuations.

5 Summary

A scaler-based counting DAQ with hardware-based particle identification was successfully implemented in the 6 GeV PVDIS experiment at Jefferson Lab. Asymmetries measured by the DAQ follow Gaussian distributions as expected from purely statistical measurements. Particle identification performance of the DAQ were measured and corrections were applied to the data on a day-to-day basis. The overall pion contamination in the electron sample was controlled to approximately 2×10^{-4} or lower, with an electron efficiency above 91% throughout the experiment. The DAQ deadtime was evaluated from a full-scale timing simulation and contributes an approximately 0.2% uncertainty to the final asymmetry results. The systematic uncertainties from the pion contamination and the counting deadtime are therefore both negligible compared to the $(3-4)\%$ statistical uncertainty and other leading systematic uncertainties. Results presented here demonstrate that accurate asymmetry measurements can be performed with even higher event rates or backgrounds with this type of scaler-based DAQ.

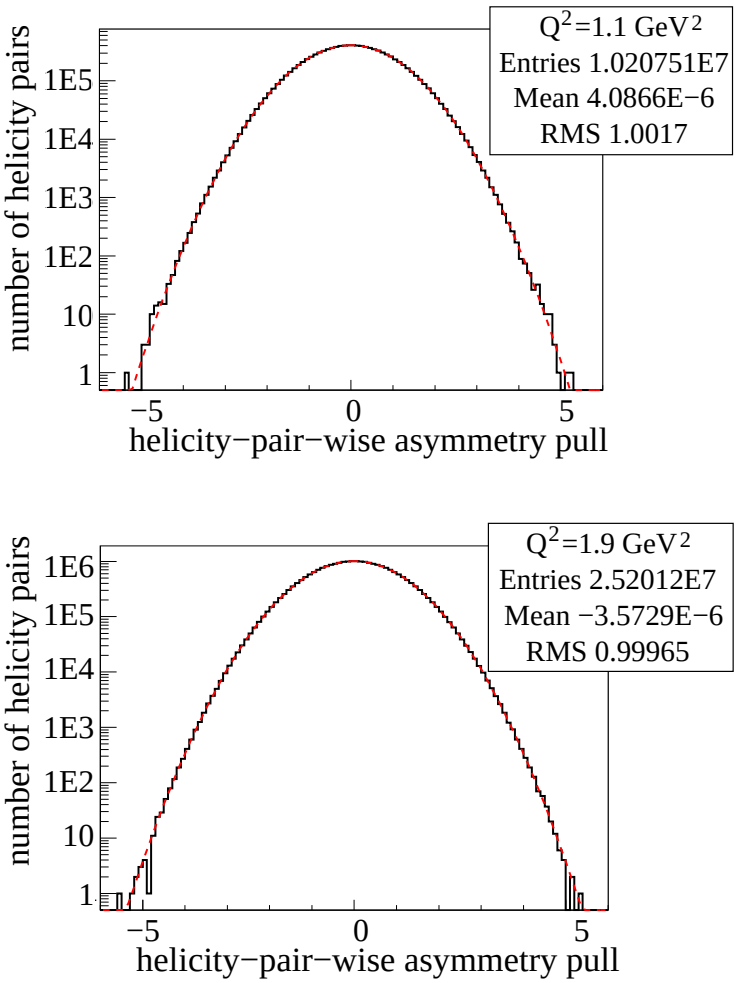

Fig. 12. [*Color online*] Pull distribution [Eq.(4)] for the global electron narrow trigger for $Q^2 = 1.1$ (top) and $Q^2 = 1.9$ (GeV/c)^2 (bottom).

Acknowledgments

This work is supported in part by the Jeffress Memorial Trust under Award No. J-836, the U.S. National Science Foundation under Award No. 0653347, and the U.S. Department of Energy under Award No. DE-SC0003885. **Notice:** Authored by Jefferson Science Associates, LLC under U.S. DOE Contract No. DE-AC05-06OR23177. The U.S. Government retains a non-exclusive, paid-up, irrevocable, world-wide license to publish or reproduce this manuscript for U.S. Government purposes.

References

[1] JLab experiment E08-011 (previously E05-007), R. Michaels, P.E. Reimer and X.-C. Zheng, spokespersons.

[2] R. Subedi *et al.*, AIP proceedings of the 18^{th} International Spin Physics Symposium (2009) 245.

[3] A publication about the E08-011 physics asymmetries is in preparation.

[4] K. Nakamura *et al.* [Particle Data Group], J. Phys. **G37**, 075021 (2010).

[5] J. Alcorn *et al.*, Nucl. Instrum. Meth. **A522** (2004) 294.

[6] R. Hasty *et al.* [SAMPLE Collaboration], Science **290**, 2117 (2000).

[7] K. A. Aniol *et al.* [HAPPEX Collaboration], Phys. Rev. C **69**, 065501 (2004).

[8] A. Acha *et al.* [HAPPEX Collaboration], Phys. Rev. Lett. **98**, 032301 (2007).

[9] K. A. Aniol *et al.* [HAPPEX Collaboration], Phys. Rev. Lett. **96**, 022003 (2006).

[10] K. A. Aniol *et al.* [HAPPEX Collaboration], Phys. Lett. B **635**, 275 (2006).

[11] Z. Ahmed *et al.* [HAPPEX Collaboration], Phys. Rev. Lett. **108**, 102001 (2012).

[12] S. Abrahamyan, Z. Ahmed, H. Albataineh, K. Aniol, D. S. Armstrong, W. Armstrong, T. Averett and B. Babineau *et al.*, Phys. Rev. Lett. **108**, 112502 (2012).

[13] C.Y. Prescott *et al.*, Phys. Lett. **B77** (1978) 347.

[14] C.Y. Prescott *et al.*, Phys. Lett. **B84** (1979) 524.

[15] F. E. Maas *et al.* [A4 Collaboration], Q**2 = 0.230-(GeV/c)**2," Phys. Rev. Lett. **93**, 022002 (2004).

[16] F. E. Maas, K. Aulenbacher, S. Baunack, L. Capozza, J. Diefenbach, B. Glaser, T. Hammel and D. von Harrach *et al.*, **2 = 0.108 (GeV/c)**2," Phys. Rev. Lett. **94**, 152001 (2005).

[17] S. Baunack, K. Aulenbacher, D. Balaguer Rios, L. Capozza, J. Diefenbach, B. Glaser, D. von Harrach and Y. Imai *et al.*, Phys. Rev. Lett. **102**, 151803 (2009).

[18] D. H. Beck, Phys. Rev. D **39**, 3248 (1989).

[19] D. S. Armstrong *et al.* [G0 Collaboration], Phys. Rev. Lett. **95**, 092001 (2005).

[20] D. Androic *et al.* [G0 Collaboration], Phys. Rev. Lett. **104**, 012001 (2010).

[21] D. Marchand, J. Arvieux, G. Batigne, L. Bimbot, A. S. Biselli, J. Bouvier, H. Breuer and R. Clark *et al.*Nucl. Instrum. Meth. A **586**, 251 (2008).

[22] D. Androic *et al.* [G0 Collaboration], Nucl. Instrum. Meth. A **646**, 59 (2011).